Engineering Structures 195 (2019) 299–308

Contents lists available at ScienceDirect

Engineering Structures

journal homepage: www.elsevier.com/locate/engstruct

Modeling techniques for post-tensioned cross-laminated timber rocking walls

Alex W. Wilson, Christopher J. Motter, Adam R. Phillips*, J. Daniel Dolan

Department of Civil and Environmental Engineering, Washington State University, Pullman, WA 99164, United States

1. Introduction

Cross-laminated timber (CLT) has migrated from its European origins in the early 1990's to North America and is gaining interest as an alternative to typical building materials, such as steel and concrete, in low- to mid-rise buildings. CLT is a mass timber product that is produced by laminating layers of precisely dimensioned lumber in perpendicular orientations to form a panel that may be used in floors or walls. Relative to glued-laminated timber (GLT), where all boards are oriented in the same direction, CLT offers the benefit of improved two-way strength and dimensional stability from shrinking and swelling [1]. CLT has significant environmental benefits over concrete and steel in terms of carbon emissions and forestry health [2]. CLT also has good fire resistance with the use of appropriate adhesives [3]. Some of the first CLT buildings in the U.S., such as Peavy Hall at Oregon State University, are in locations with high seismic demand. The seismic force resisting system in this building consisted of CLT rocking walls coupled by energy dissipation devices. However, this system is not classified as a standard seismic force resisting system in U.S. building codes. FEMA P-695 [4], a code prequalifying procedure, requires extensive numerical modeling to demonstrate system performance and reliability, which is impractical for typical project timelines. Engineers can alternatively use performance-based seismic design to obtain jurisdiction approval, which similarly requires numerical modeling, but the number of analyses required is reduced when compared to the FEMA procedure.

Practical modeling techniques for CLT rocking walls are needed to conduct nonlinear time-history analyses required for performance-based seismic design, and these models could be an option for use with future code-based design. Despite this need, there is currently a lack of research on practical nonlinear modeling of CLT rocking walls. This paper presents the development and validation of two modeling methods. One method utilizes a high-order approach that allows detailed assessment of local stress and crushing behavior, as well as investigation into parameters governing the moment-rotation behavior. The second method utilizes a computationally-efficient reduced-order approach for assessment of building responses in time-history analyses, and this approach is convenient for use with separately characterized hysteretic damping devices. While the higher-order model could be used to analyze a complete building, the computational power and time required for analysis would make this option unmanageable. Both modeling approaches were validated against experimental tests. In addition, a parametric study was conducted for both modeling approaches to assess the impact of variation in wall length and initial post-tensioning force on wall response.

2. Background and literature review

CLT rocking wall systems typically utilize hysteretic damping devices and may include self-centering provided by post-tensioning tendons or self-centering dampers at the base of the wall (e.g., the friction dampers studied by Hashemi et al. [5]). Adjacent walls may be coupled using hysteretic damping devices, such as U-shaped flexural plates (UFPs) (Kelly et al. [6]; Buchanan et al. [7]), friction dampers (Hashemi et al. [8]), or plywood sheets (Iqbal et al. [9]). For post-tensioned (PT) CLT walls coupled with hysteretic damping devices, shown in Fig. 1, seismic lateral forces (indicated as F in Fig. 1) may cause the panels to "rock", which leads to deformation (indicated as Δ_v in Fig. 1) in the hysteretic energy dissipation devices that are located between the panels. The dissipation devices provide supplemental damping to the system and coupling forces that increase the system stiffness and global overturning moment resistance. In addition, these devices are easily replaceable after an earthquake event if they incur significant damage. The CLT rocking walls are post-tensioned using vertical rods that are located at the wall centerlines and are either internal in a small cavity down the center of the wall panel or external along the outside faces. The rods are anchored at the top of the wall and at the foundation using typical steel anchorage supports for PT systems.

The decompression moment is defined as the overturning moment that initiates uplift (i.e. rocking) at a wall corner and is a function of the initial PT force (T_i) and self-weight (W) of the wall. When the overturning moment demand exceeds the decompression moment, the bottom corner of the wall lifts off the foundation and moment resistance is provided by a force couple created between the PT rod(s) and the resultant compression force at the toe in contact with the foundation (indicated as T and C in Fig. 1, respectively). During rocking, sliding is

* Corresponding author.
E-mail addresses: alex.w.wilson@wsu.edu (A.W. Wilson), c.motter@wsu.edu (C.J. Motter), a.phillips@wsu.edu (A.R. Phillips), jddolan@wsu.edu (J.D. Dolan).

https://doi.org/10.1016/j.engstruct.2019.06.011
Received 27 November 2018; Received in revised form 31 May 2019; Accepted 5 June 2019
Available online 10 June 2019
0141-0296/

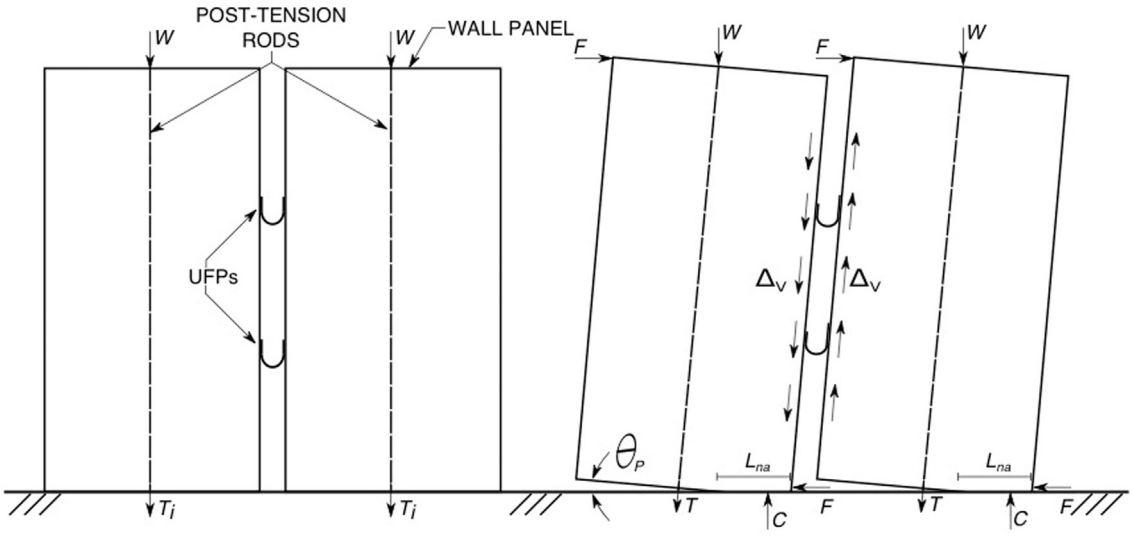

Fig. 1. Coupled Rocking Wall without Lateral Deformation (Left) and Free-Body Diagram of Rocking Wall with Lateral Deformation (Right).

prevented by a combination of friction forces and shear transfer devices at the corners. The rocking action results in elongation of the PT rod(s) and nonlinear response at the toe of the wall due to crushing. Provided the PT rods have not yielded and crushing damage is not severe, the tension force in the PT rods acts as a restoring force that re-centers the wall at the end of an earthquake, minimizing residual drift of the building.

Research on rocking walls was initially conducted for reinforced concrete (e.g. Priestly et al. [10]; Perez et al. [11]; Kurama et al. [12,13]; Perez et al. [14]), later for laminated veneer lumber (LVL) (e.g. Sarti et al. [15]), and more recently for CLT (e.g. Ganey et al. [16]). Tests performed by Ganey et al. [16] provided data for CLT rocking walls with various PT forces on both flexible and rigid foundations, as well as for walls coupled with UFPs. Experimental and parametric studies by Baird et al. [17] led to improved characterization of the deformation behavior of UFPs. The authors are not aware of literature on component testing of CLT rocking walls aside from Ganey et al. [16].

Current design methods for rocking walls involve analytical procedures developed by Pampanin et al. [18] for analyzing concrete frames, further developed by Newcombe et al. [19] for timber walls, and later modified by Ganey [20], Kovacs and Wiebe [21], and Akbas et al. [22] for CLT. Newcombe [23] developed finite element models of LVL rocking walls that were shown to produce results that matched the Newcombe et al. [19] analytical procedures. Currently, published modeling approaches for CLT walls are limited to those developed by Ganey [20] and Kovacs and Wiebe [21], which utilize distributed plasticity (spring) models in OpenSees [24]. The Ganey [20] approach utilizes contact elements and relies on the results of experimental tests for calibration. The Kovacs and Wiebe [21] approach is based on the Winkler Spring Analogy, which relies on material properties for spring definitions rather than experimental data. Both techniques were shown to produce results that match well with experimental data. However, the approaches do not enable assessment of crushing behavior, a parameter of interest in resiliency assessments and development of alternate/enhanced panel layups. Additionally, these approaches were developed for use in OpenSees [24], which is more often used by researchers than practitioners. To address these issues, this paper presents a reduced-order lumped plasticity approach that may be implemented into a broader range of analysis applications and programs for PT CLT rocking walls.

3. Experimental test summary

The modeling approaches presented below are applicable to CLT rocking walls on stiff foundations that exhibit no PT bar yielding for all levels of shaking. Both of these conditions are expected in practice, with the latter needed to ensure self-centering. The models are applicable for in-plane wall response and do not consider bi-directional lateral deformation. The models are validated with test results of CLT rocking walls conducted by Ganey et al. [16]. The experimental program conducted by Ganey et al. [16] consisted of seven rocking walls with variation in initial PT forces, panel materials, boundary conditions, and/or the use of energy dissipation devices (UFPs). Of the seven specimens, Specimen 2 and Specimen 6 were used for model validation, as these specimens were CLT walls on stiff foundations without PT yielding at drifts below 5% and 4%, respectively. Specimen 1 was also a CLT wall on a stiff foundation without PT bar yielding; however, Specimen 1 contained pre-test damage and experienced significant delamination at early drift cycles, affecting the reliability of the results. For Specimen 3b and Specimen 3c, yielding of the PT rod occurred at approximately 3% and 3.5% drift, respectively. Specimen 4 was tested on a flexible (CLT) foundation, and Specimen 5 consisted of a structural composite lumber (SCL) core.

Specimen 2, illustrated in Fig. 2a, was an individual CLT panel with a 0.17 m by 1.22 m rectangular cross-section and was constructed using two Hem-Fir 5-ply panels that were spliced together with steel plates and 6.35 mm SDS screws. The wall was 4.43 m tall, and a quasi-static cyclic displacement protocol was applied 4.07 m above the base of the wall during testing. A 36 mm PT rod tensioned to an initial force of 109kN ran through an internal cavity down the centerline of the panel. The wall was restrained against out-of-plane displacement at the bottom and at a height of 3 m on both sides of the wall. Shear force was transferred at the bottom of the wall through steel angles that were welded to the foundation beam [20].

Specimen 6, illustrated in Fig. 2b, consisted of two adjacent CLT walls coupled by hysteretic energy dissipation devices (UFP connectors) and was used to validate the reduced-order model for coupled CLT rocking walls. The walls, measuring approximately 0.17 m by 1.2 m by 4.85 m, each consisted of two 5-ply Hem-Fir CLT panels and were coupled using two UFP connectors, one at one-third and the other at two-thirds the height of the wall panel, that were connected to the walls with timber rivets. The steel UFPs had a width, thickness, and bend diameter of 10.2 cm, 0.95 cm, and 10.3 cm, respectively. The yield and ultimate strength of the steel utilized for the UFPs were 414 MPa and

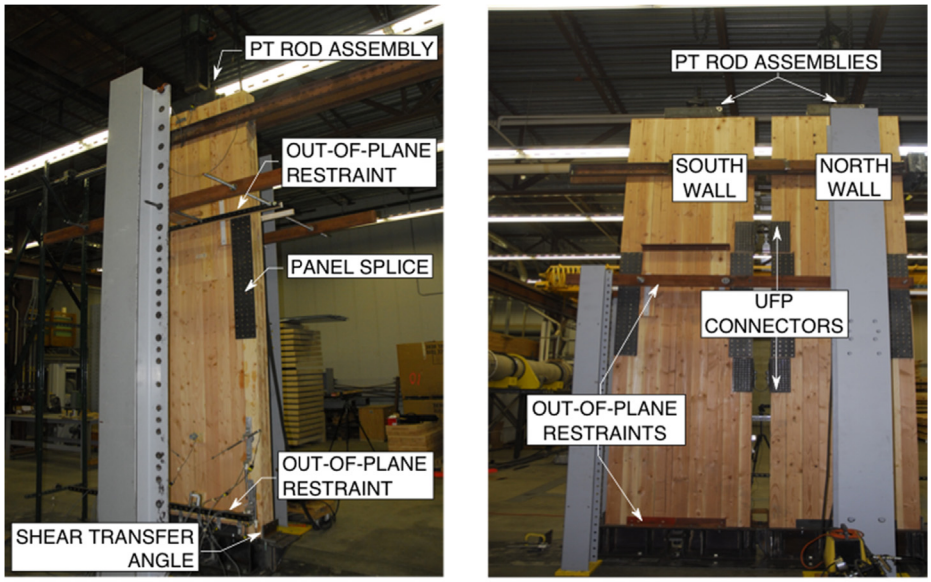

(a) Specimen 2 (b) Specimen 6

Fig. 2. Test Set-Up for (a) Specimen 2 and (b) Specimen 6 [20].

593 MPa, respectively. For Specimen 6, the PT rods were 31.75 mm in diameter and had an initial PT force of 334 kN and 378 kN for the North and South wall, respectively. Specimen 2 and Specimen 6 were subjected to an identical displacement protocol and had consistent boundary conditions [20].

4. High-order model

4.1. Model characterization

The high-order model for CLT rocking walls is a finite element model that was developed and calibrated to Specimen 2 from Ganey et al. [16]. The high-order model was developed to investigate local effects and behavior of a given rocking wall configuration, including local crushing behavior at the wall toes, stress distribution throughout the wall, moment-rotation characteristics, as well as for validation of reduced-order models that are more practical for conducting nonlinear time-history analyses of buildings. The model was constructed using the commercially available structural analysis software SAP2000 [25], but the modeling techniques utilized within the program may be implemented into a wide variety of other analysis programs.

In the high-order model, illustrated in Fig. 3a, four-node shell elements were used for the CLT panel, a multi-linear plastic link element was used for the PT rod, and multi-linear elastic link elements were used for the PT anchorage, steel wide-flange beam foundation, and angles utilized for shear transfer. The orthotropic material properties of the shell elements were obtained from material tests performed by Ganey et al. [16] and are provided in Table 1. Experimental compression tests were performed to determine the nonlinear stress-strain relationship of the panel after crushing at the toe [16,26]. This behavior was idealized as elastic-perfectly-plastic, as illustrated in Fig. 4a, and was used to characterize the inelastic compression behavior of the CLT. A strain capacity of 0.02 was used to avoid extrapolating beyond the extent of the test data. The majority of the wall remains elastic during rocking, while only the corners (approximately 30 × 46 cm) and the portion beneath the PT anchorage box (approximately 56 × 15 cm) may experience inelastic behavior, as illustrated in Fig. 3a. Therefore, two mesh sizes of shell elements were used. The middle section of the wall used an elastic material relationship and was meshed using 150 mm by 150 mm shell elements. The sections at the wall corners and beneath the PT anchorage box used the nonlinear CLT material shown in Fig. 4a and were meshed using 25.4 mm by 25.4 mm shell elements.

The PT rod assembly was modeled using two components: the PT rod and the anchorage box-to-CLT wall connection. The PT rod was modeled using an axial-only multi-linear plastic link element. One end of the PT link element was attached to the center of the rigid beam and the other end was attached to a pinned node beneath the base of the wall, as illustrated in Fig. 3a. The material properties for the PT rod were taken from material tests performed by Ganey et al. [16], illustrated in Fig. 4b and provided in Table 1. Kinematic hardening was assumed for the cyclic behavior. The PT anchorage box, as illustrated in Figs. 2 and 3a, was modeled utilizing a rigid beam and multi-linear elastic link element assembly. The 56 cm long rigid beam rested on multi-linear elastic link elements that were attached to the shell elements at the top of the wall.

The effective PT force (i.e., the PT force at 0% drift) at a given drift decreased with each additional drift cycle, which was not explicitly characterized in the high-order model. Instead, this was addressed by utilizing the PT force coinciding with 4% drift during the experimental test, approximately 59.2 kN (originally 109 kN), corresponding to 54% of the original force, which better targets the PT force experienced during rocking. This value represented the average of the effective PT forces experienced by Specimen 2 for the drift cycles assessed in this study. The initial PT force was achieved by applying a displacement to the bottom of the PT link at its pinned boundary condition.

The stiff steel boundary conditions at the base of the panel were represented with a series of elastic link elements. To properly model rocking, these elements had zero tensile stiffness and a compressive stiffness that was 10^6 times that of CLT to concentrate all deformation into the shell elements. These springs were distributed along the bottom of the panel and at the sides of the bottom corners to represent the steel angles. A planar analysis was conducted, as it was assumed that out-of-plane displacements were negligible due to the out-of-plane restraints used during the test, shown in Fig. 2a.

The analysis was conducted by first applying the dead load and initial PT force to the panel and then executing a reversed cyclic lateral displacement protocol using a direct integration solution routine. The protocol used by Ganey et al. [16] was created based on ACI ITG-5.1-07 [27]. The protocol used for the model consisted of three cycles at drifts of 0.6%, 1.35%, 2%, 3%, 4%, and 5%, which matched the peak drifts used by Ganey et al. [16] with the following exceptions: cycles at 0.4% or less were omitted because these cycles did not result in any

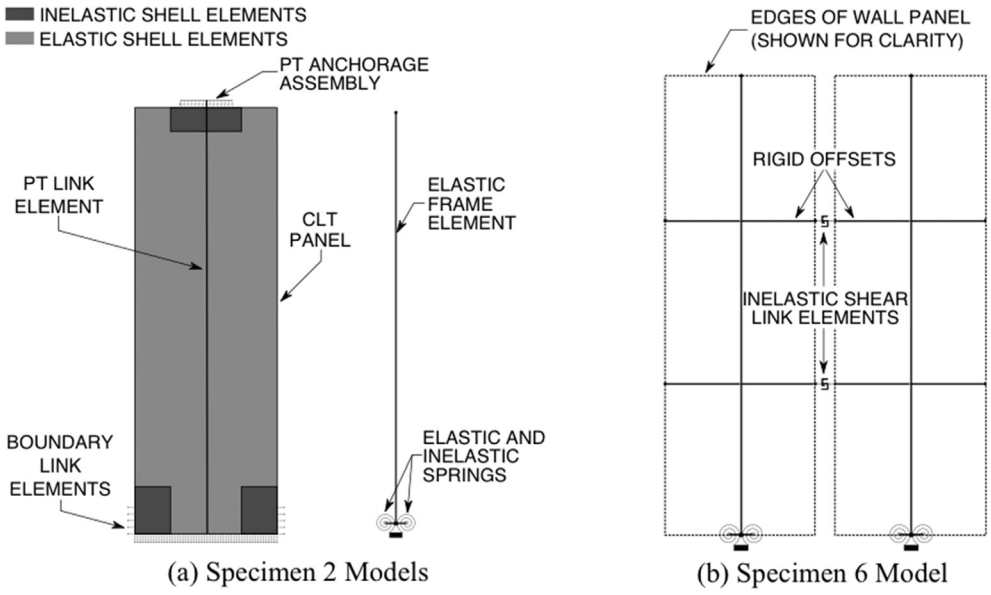

Fig. 3. (a) High-Order and Reduced-Order Model of Specimen 2 and (b) Reduced-Order Model of Specimen 6.

Table 1
Material Properties for Specimen 2 used in High-Order Model.

Material Type	Property[1]	Value
CLT Material	E_1	2828 MPa
	E_2	2080 MPa
	E_3	901 MPa
	G_1, G_2, G_3	345 MPa
	ν_1, ν_2, ν_3	0.3
	F_y	24.8 MPa
PT Rod (Specimen 2)	E	221 GPa
	F_y	911 MPa
	F_u	1030 MPa
	E_H[2]	19.6 MPa
PT Rod (Specimen 6)	E	221 GPa
	F_y	929 MPa
	F_u	1091 MPa
	E_H[2]	19.6 MPa

[1] The local 1, 2, and 3 directions of the panel coincide with the length, height, and thickness, respectively.
[2] Strain hardening modulus.

compression yielding of CLT at the toe of the wall, and cycles above 5% were omitted because variability and imperfections in CLT that were not characterized in the model became more pronounced.

4.2. Model assessment

In the positive loading direction, the moment-deformation response determined using the model closely matched the test, as shown in Fig. 5a, and captured the low decompression moment and high decompression stiffness. As shown in Fig. 5b, the PT rod response from the model in the positive loading direction closely matched the test between 1.35% and 4% drift and was slightly lower at drifts less than 1.35% and slightly higher at drifts greater than 4% due to the initial force applied to the PT rod in the model, as explained previously. In the negative loading direction, the model did not match the experimental test behavior because the experimental specimen delaminated during testing. Delamination resulted in effective resistance lower than design resistance in the negative direction, consistent with the asymmetric hysteretic behavior shown in Fig. 5a. Premature delamination of the test specimen was most likely a result of the quality of laminations utilized during laboratory fabrication, which would not have been present for production CLT panels that conform to the PRG-320 manufacturing standard [28]. In addition, resistance loss was also attributed to loss in effective PT force during reversed-cyclic loading, as described previously. For these reasons, all subsequent comparisons between the high-order model and test of Specimen 2 will be referring only to the positive direction cycles.

Comparisons between the model and test are provided in Table 2 for values of base moment (M_{model} and M_{test}, respectively), stiffness (K_{model}

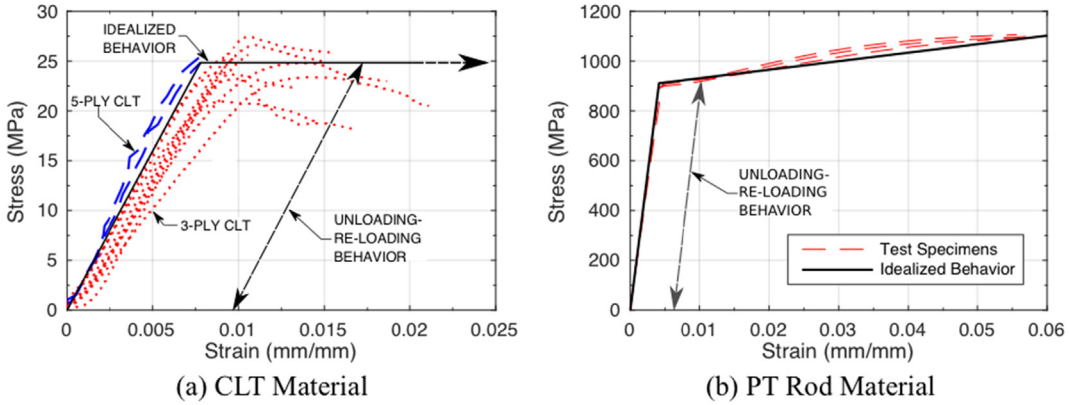

Fig. 4. Stress-Strain Behavior of: (a) CLT in Compression and (b) Post-Tensioning Rod in Tension [16].

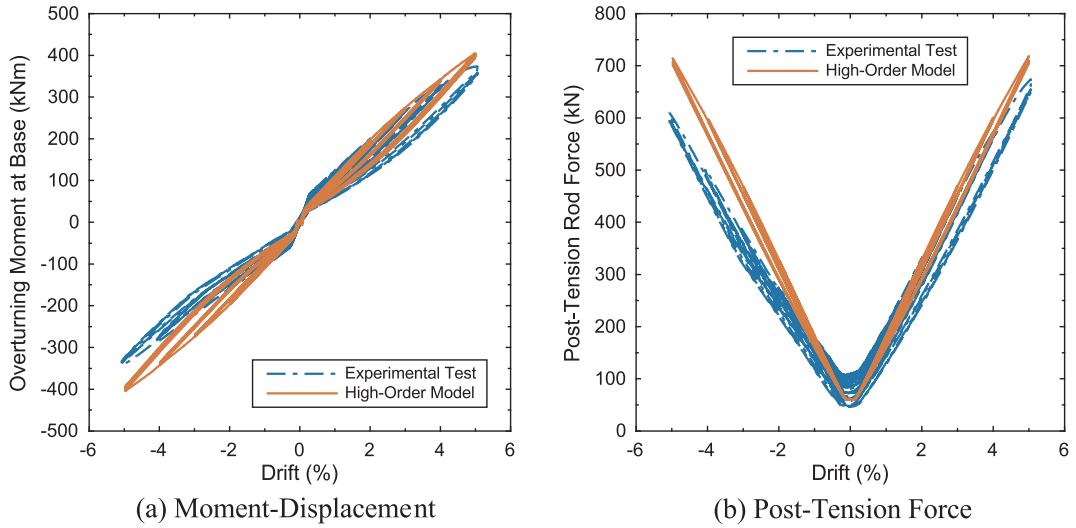

Fig. 5. Test and High-Order Model (a) Moment-Displacement and (b) Post-Tension Force.

and K_{test}, respectively), and PT force (T_{model} and T_{test}, respectively) for the first cycle at each drift level. Stiffness was determined from the moment-rotation response as the effective secant stiffness from the origin to the point at peak drift in a cycle. For drifts at and between 1.35% and 4%, the absolute error between the experimental test and the model for peak moment (M_{Error}), stiffness (K_{Error}), and PT force (T_{Error}) was within 6.8%. The absolute error increased to 8.3% at 5% drift because the initial PT force applied to the model was higher than the effective PT force experienced at 5% drift for the test. At 0.6% drift the absolute error was also larger at 20.3% due to the lower initial PT force applied to the model.

A critical parameter for the reduced-order model is the amount of rotation experienced at the bottom of the wall, which is directly correlated to the amount of heel uplift and toe crushing. For the high-order model to be a useful calibration and validation tool for the reduced-order model, this behavior must be accurately captured. The left heel uplift for the high-order model (LHU_{model}) and experimental test (LHU_{test}) are provided in Table 3, along with their respective errors (LHU_{Error}). The uplift behavior obtained from the model at the left heel, which corresponds with the positive moment direction, matches well with the experimental test. This demonstrates that the rocking action occurring in the model is very similar to the behavior occurring during the test.

Although no test data exists for comparison, the high-order model may be utilized to investigate stress distributions and local crushing deformation at the wall toes. After the initial PT force is applied, most of the wall is in compression, with a maximum compressive stress of approximately 0.634 MPa exhibited beneath the PT anchorage at the top of the wall, as illustrated in Fig. 6a. At 3% drift, illustrated in Fig. 6b, a concentration of plastic strain at the toe of the wall, as well as an increase in compressive stress throughout the wall panel is exhibited. At the toe, approximately 3100 cm^3 (peak height of 18 cm and contact area of 206 cm^2) of timber experiences plastic behavior, corresponding to a stress equal to or greater than 24.8 MPa. Fig. 6b also illustrates that this plastic compressive stress propagates more rapidly in the vertical direction (along the height of the panel) than the horizontal direction (along the width of the panel) with increase in drift. By utilizing results of the reduced-order model (presented in the next

Table 3
Heel Uplift for Test and High-Order Model for Specimen 2.

Drift[1]	LHU_{model} (mm)	LHU_{test} (mm)	LHU_{Error} (%)
0.60%	2.8	4.3	54.5
1.35%	9.6	11.4	19.4
2%	16.0	17.4	9.3
3%	25.4	26.7	5.1
4%	34.8	35.6	2.2
5%	43.7	44.0	0.6

[1] Only initial cycles of each drift target are utilized.

Table 2
Moment Resistance, Stiffness, and PT Force Comparison for Test and High-Order Model for Specimen 2.

		Moment Results			Stiffness Results			PT Force Results		
	Drift	M_{test} (kNm)	M_{model} (kNm)	M_{Error} (%)	K_{test} (kN/m)	K_{model} (kN/m)	K_{Error} (%)	T_{test} (kN)	T_{model} (kN)	T_{Error} (%)
High-Order Model	0.60%	94	75	−20.3	1129	900	−20.3	155	123	−20.7
Reduced Order Model			79	−16.1		947	−16.1		–	–
High-Order Model	1.35%	150	140	−6.8	670	625	−6.8	248	233	−6.0
Reduced Order Model			143	−4.9		−4.9	−4.9		–	–
High-Order Model	2.00%	202	197	−2.4	612	598	−2.4	334	328	−1.8
Reduced Order Model			197	−2.3		599	−2.3		–	–
High-Order Model	3.00%	272	274	1.0	549	555	1.0	460	469	1.9
Reduced Order Model			270	−0.5		546	−0.5		–	–
High-Order Model	4.00%	332	342	3.0	503	519	3.0	578	601	4.0
Reduced Order Model			340	2.4		515	2.4		–	–
High-Order Model	5.00%	374	405	8.3	453	491	8.3	674	718	6.6
Reduced Order Model			410	9.7		497	9.7		–	–

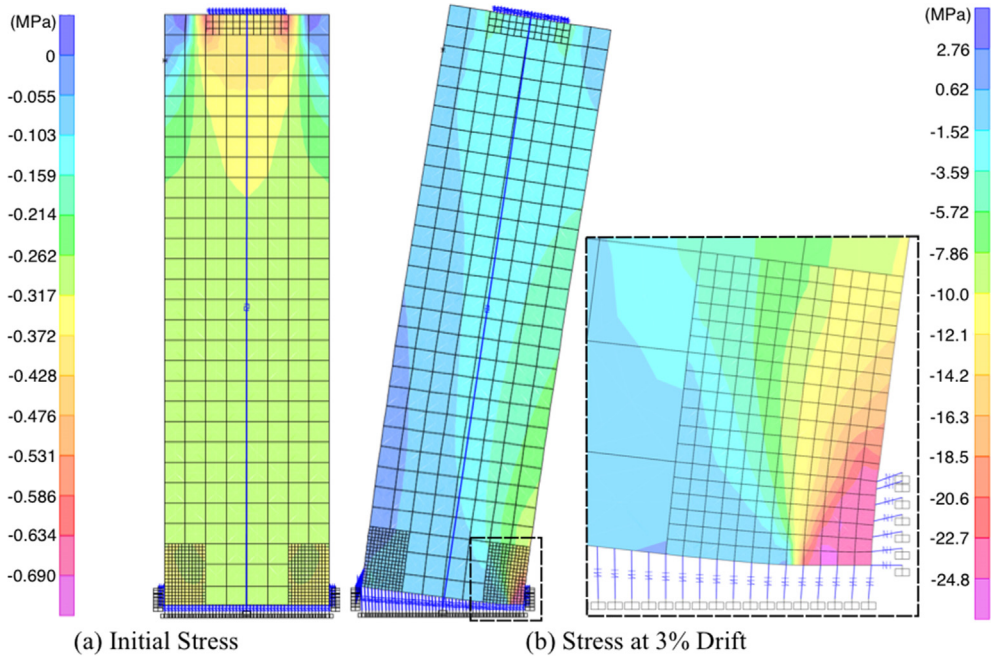

Fig. 6. Specimen 2 Vertical Wall Stress (a) After Initial PT Force is Applied and (b) At 3% Drift, with Close-Up View of Toe Stresses.

section), the exhibited damage at the toes may be approximated, allowing structural resiliency aspects to be assessed.

5. Reduced-order model

5.1. Model characterization

Implementation of the high-order rocking wall model is intended for analysis situations where accuracy in capturing the full behavior of the wall panel and base rotations are needed. As discussed above, the high-order model provides significant detail on the stresses, strains, and force distribution of the rocking wall system. This type of analysis is impractical for conducting suites of nonlinear time-history analyses of 3D buildings due to the memory requirements and long computational time. A reduced-order model, constructed of beam and link elements, was developed to accurately represent the global hysteretic response of the panel with significantly shorter computational time. For a given wall, formulation of the reduced-order model first requires formulation of a high-order model used to conduct a pushover analysis to generate a monotonic backbone curve. The time required to create the high-order model, generate a backbone curve, and characterize a reduced-order model is minimal compared to the time associated with conducting subsequent suites of time-history analyses using the high-order model.

The reduced-order model, shown in Fig. 3a, is comprised of an elastic frame element that captures the elastic deformation of the CLT wall panel and two rotational spring elements, one elastic and one nonlinear, in parallel that are located at the wall-foundation interface. The elastic spring captures the decompression resistance of the wall, while the inelastic spring captures the plastic rotation attributed to the couple between the PT force and toe crushing. The elastic frame element used the same CLT material definition as the high-order model. The elastic spring element was bilinear, as illustrated in Fig. 7a, with infinite stiffness up to the decompression moment, followed by zero stiffness after decompression. The decompression moment, M_{dec}, is determined with Eqs. (1)–(3) as:

$$M_{dec} = (T_i + W)d \quad (1)$$

$$d = L_W/2 - c \quad (2)$$

$$c \cong 1/8L_W \quad (3)$$

where d is the distance between the initial PT force and the resultant compressive force, L_W is the length of the wall panel, and c is the distance of the resultant compressive force from the edge of the wall panel, as illustrated in Fig. 8a. The distance c was rationalized by assuming a neutral axis depth of $0.375L_W$ from the edge of the wall panel and taking the resultant compressive force as one-third of that depth, consistent with assumptions made in Ganey [20].

The moment resistance versus plastic rotation (θ_p) relationship of the inelastic spring element, illustrated in Fig. 7a, was determined using results from the high-order model. The moment resistance was determined as the difference between moment resistance from the high-order model backbone and the decompression moment, since the decompression moment was incorporated into the elastic spring. The combined resistance of the elastic and inelastic spring provides the resistance of the high-order model, as illustrated in Fig. 7a. For a given wall drift, the plastic rotation, illustrated in Fig. 8a, for the inelastic spring was determined with Equation (4) as:

$$\theta_P = \delta_{toe}/(L_W - L_{na}) \quad (4)$$

where δ_{toe} is the uplift at the heel and L_{na} is the neutral axis depth. The neutral axis depth, which represents the required wall-foundation contact length to balance the tension (T) and compression (C) forces, and uplift at the toe may be determined directly from the high-order model at a given drift magnitude (Δ_S), as illustrated in Fig. 8a.

The determination of θ_p in Eq. (4) differs from the analytical method used by Ganey [20] and shown in Eq. (5).

$$\theta_P = (\delta_d/h_w) - [M/(k_w h_w^2)] \quad (5)$$

where δ_d is the lateral wall displacement at a specific drift level, M is the applied moment, k_w is the combined flexural and shear stiffness of the wall, and h_w is the height of the wall. Eq. (5) uses a simplifying assumption that the elastic deformation is constant after decompression which results in plastic rotation values being larger than those computed with Eq. (4). Modifying Eq. (5) to account for the change in elastic deflection that occurs with changes in drift is cumbersome. Eq. (4) addresses the issue by enabling explicit determination of plastic rotation.

The inelastic spring was modeled in SAP2000 utilizing a pivot hysteresis type that allowed unloading behavior to be controlled. Dowell et al. [29] provides a detailed explanation of the development

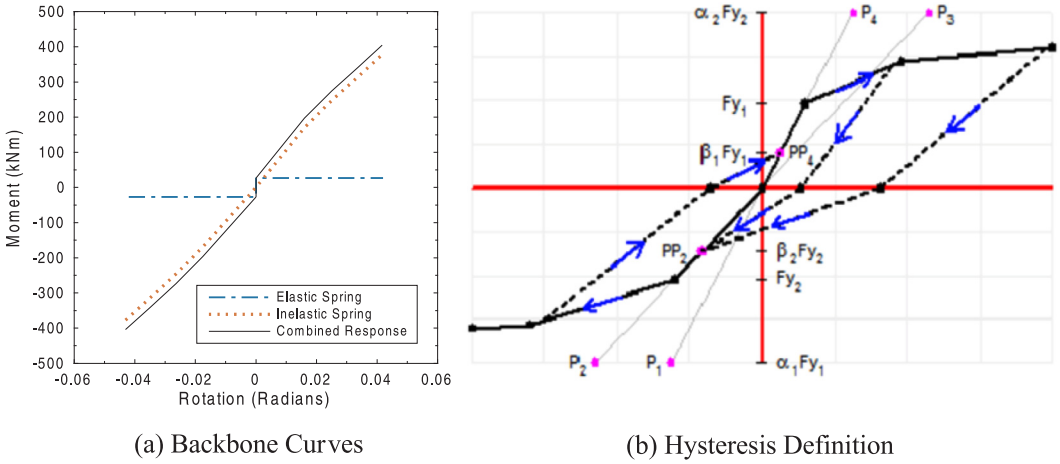

Fig. 7. (a) Elastic, inelastic, and combined (elastic and inelastic) spring backbone curves for Reduced-Order Specimen 2 model, (b) Pivot hysteresis model used in SAP for inelastic spring [25].

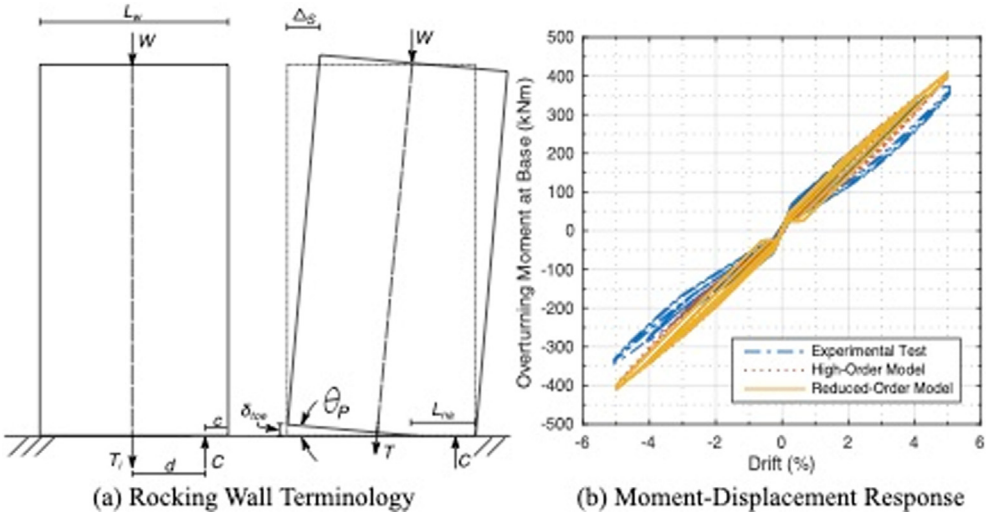

Fig. 8. (a) Rocking Wall Terminology for Reduced-Order Model Creation and (b) Specimen 2 Moment-Displacement Response from Test, High-Order Model, and Reduced-Order Model.

and behavior of this hysteresis model. This hysteresis type was selected because it allowed better control over the loading and unloading behavior compared to the other hysteretic types available in SAP2000. Additionally, Dowell et al [29] demonstrated strong fit between this hysteresis model and measured data for reinforced concrete columns. As illustrated in Fig. 7b, this hysteresis type utilizes α_1, α_2, β_1, and β_2 parameters, which define the pivot points for unloading from positive yield force to zero, unloading from negative yield force to zero, loading from zero to positive yield force, and loading from zero to negative yield force, respectively. All of these parameters were set to zero to best match the pinching shape observed in the system response of the high-order model. In addition, a parameter η is utilized in the hysteresis definition to define the amount of degradation of the elastic slope after inelastic deformation has been experienced by the element. η was also set to zero, since significant degradation did not occur.

The elastic and inelastic springs allow the reduced-order model to capture flag-shaped hysteretic behavior caused by the decompression moment. Note that the flag-shaped hysteresis is not very pronounced for Specimen 2 due to the low magnitude of the decompression moment relative to the maximum moment attained during the test.

5.2. Model assessment

Moment resistance (M_{model}) and stiffness (K_{model}) results from the reduced-order model, high-order model, and the experimental test are provided in Fig. 8b and Table 2. For cycles between 1.35% and 4% drift in the positive loading direction, the absolute errors for the reduced-order model compared to the test did not exceed 4.9%, while the absolute errors for the high-order model compared to the test did not exceed 6.8%. This level of error was deemed acceptable, given that the determination of moment resistance and stiffness is dependent on behavior at the compression toe. Both models were deemed to adequately capture the experimental moment resistance and stiffness within design level drift limitations. In addition, because the reduced-order model is characterized from moment and rotation results of the high-order model, results explicitly determined from the reduced-order model (e.g., moment at the base) may be linked back to the high-order model to estimate crushing damage for resiliency assessment.

6. Coupled wall model

6.1. Model development

Crushing at the toe of rocking walls does not dissipate a significant

amount of energy, as evidenced by the hysteretic loops in Fig. 5a. To preserve the self-centering capability of the system, the PT bar(s) must remain elastic during rocking. This design greatly minimizes the amount of energy dissipated by the CLT walls alone. The use of UFPs, or other energy dissipating couplers attached between adjacent walls, add moment resistance, stiffness, and energy dissipation to rocking wall systems.

Results from the reduced-order model were compared with test results from Specimen 6 [16] to consider walls coupled with UFPs. As shown in Fig. 3b, the model for Specimen 6 consisted of two reduced-order wall models with rigid frame offsets to the edges of the wall panels. The rigid offsets were coupled with an inelastic shear link element with the force-deformation characteristics of the UFP utilized for the test. The reduced-order wall models were formulated using the methodology described in the previous section, which requires formulation of a high-order model to develop the reduced-order model.

The high-order model was characterized using the same techniques as Specimen 2. Material properties were taken as average values obtained from material tests from Ganey et al. [16], as provided in Table 1. The PT rod diameter was 31.75 mm. The initial PT force for the North and South wall specimens were 334kN and 378kN, respectively, and only 10% of this force was lost throughout the duration of the test. A monotonic pushover of each wall was performed to 4% drift to determine the backbone curve using the high-order model. A maximum of 4% drift was targeted because higher drifts resulted in yielding of the PT rods, which was not a parameter of interest in this study.

The UFP was characterized with an inelastic shear link that contained the force-deformation characteristics of the UFP link tested by Ganey [20]. Utilizing the raw test data, force-displacement data points were obtained from the UFP backbone curve. The link was fixed for all degrees of freedom, except the vertical shear direction, which was characterized using the force-displacement data points obtained from the UFP backbone curve and a kinematic strain hardening hysteretic behavior.

6.2. Model assessment

The reversed-cyclic loading protocol used by Ganey [20] for testing the UFP was used in the model to compare the hysteretic response of a single UFP. The force-deformation hysteretic response of the shear link element obtained from the model matched well with that of the experimental test, as evident in Fig. 9a. The cumulative dissipated energy for all cycles was 111 kNm for the test and 108.3kNm for the model, resulting in a −2.43 percent error between the model and the test.

Table 4
Moment Resistance for Test and Reduced-Order Model for Specimen 6.

Drift	Direction	M_{model} (kNm)	M_{test} (kNm)	M_{Error} (%)
0.60%	+	357	380.5	−6.2
1.35%	+	558	604.8	−7.7
2%	+	687.2	699.8	−1.8
3%	+	810.4	792.6	2.2
4%	+	896.4	839.9	6.7
5%	+	950.4	870.5	9.2

Force-deformation hysteretic response for the test and the coupled reduced-order model are shown in Fig. 9b, with the total base moment (i.e., sum of base moments for both walls) at the first cycle of each drift target (M_{model}, M_{test}) provided in Table 4. In the negative direction, discrepancies between model and test results exist due to early delamination of the South wall during small drift cycles, consistent with the abrupt drop in moment resistance between 0% and −1% drift evident in Fig. 9b. Just as for Specimen 2, the model is not able to capture material defects associated with delamination, which is not expected to occur for panels that conform to the PRG-320 manufacturing standard [28]. Therefore, comparisons focus on the positive loading direction. For positive drift cycles not exceeding 4% drift, the maximum absolute error in moment resistance (M_{Error}) between the test and model at the first cycles of each drift target was 7.7%. Values for the dissipated energy of the first cycle at each drift level are provided in Table 5 for the model (W_{model}) and the test (W_{test}). The error for the model compared to the test ranged from 1.8% to 11% for drifts of 1.35% and 4%. This level of accuracy indicates that the reduced-order model is capable of capturing the global response of CLT rocking walls coupled with UFPs.

7. Parametric study

A parametric study on uncoupled CLT rocking walls was performed to understand the influence that variation in design parameters have on behavior of the wall. Initial PT forces of 445 kN, 890 kN, 1335 kN, 1779 kN, and 2224 kN were used in combination with wall lengths of 1.83 m, 2.44 m, 2.74 m, and 3.04 m, resulting in 20 different configurations. The range of PT forces and wall lengths are intended to encompass the practical lower and upper bounds for low- and mid-rise buildings. Each wall in the parametric study was subjected to a single cycle at 0.5%, 1%, 2%, 3%, 4%, and 5% drift. The PT rods were designed to remain elastic to ensure that the restoring force provided re-centering.

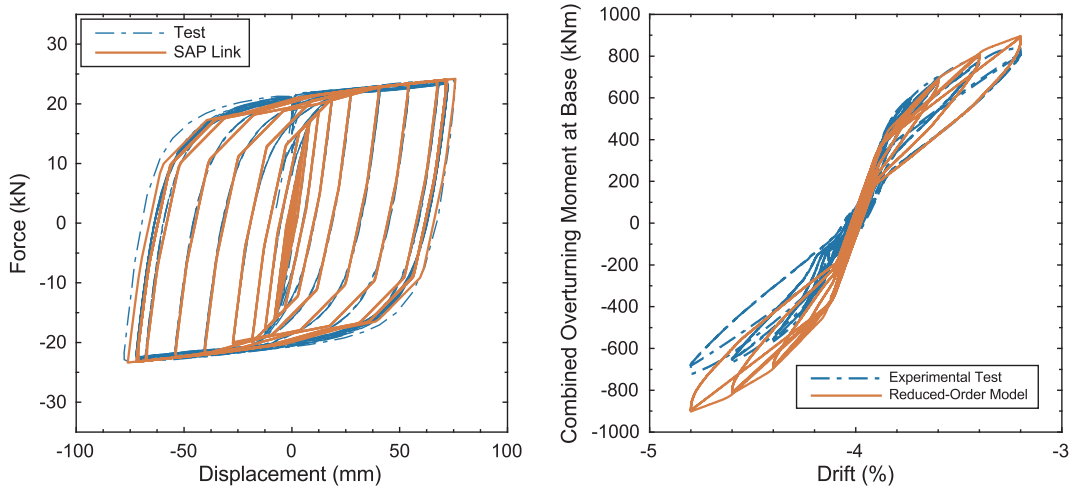

(a) UFP Force-Deformation Response (b) Moment-Displacement

Fig. 9. (a) Force-Deformation Response of UFP from Test and SAP2000 Model and (b) Specimen 6 Force-Deformation Response from Test and Reduced-Order Model.

Table 5
Dissipated Energy for Test and Reduced-Order Model for Specimen 6.

Drift	W_{model} (kNm)	W_{test} (kNm)	W_{Error} (%)
0.6%	22	18	25.5
1.35%	138	135	1.8
2.0%	302	288	4.9
3.0%	709	639	11.0
4.0%	1162	1051	10.5

Table 6
Material Properties for Parametric Study.

Material	Property	Value
CLT	E_1	4218 MPa
	E_2	5273 MPa
	E_3	938 MPa
	G_1	219 MPa
	G_2	174 MPa
	G_3	451 MPa
	ν_1, ν_2, ν_3	0.3
	F_y	37000 kPa
PT Rod	E	200 GPa
	F_y	880 MPa
	F_u	1030 MPa
	E_H[2]	19.6 MPa

[1]The local 1, 2, and 3 directions of the panel coincide with the length, height, and thickness, respectively.
[2] Strain Hardening Modulus.

For each wall in the parametric study, a high-order and reduced-order model was created using the techniques presented in the paper. To be consistent with current manufacturing standards and panel dimensions, Structurlam's [30] V2M1.1 panel was selected, with the panel oriented in the strong direction (i.e., longitudinal layers oriented in the vertical direction). The panel was assumed to be Lodgepole Pine from the Spruce-Pine-Fir (SPF) species group. Material properties provided in Table 6 were determined from FPL [31]. It was assumed that only the parallel layers would contribute to crushing and flexural and shear stiffness. This resulted in an effective flexural and shear modulus of 56% and 44% of the original values in the horizontal (local 1) and vertical (local 2) direction, respectively. Material properties utilized for the PT rod were taken from Dywidag [32] for 46 mm PT rods. For each model, 4PT bars were idealized as one link.

Values of maximum moment resistance at 0.5%, 1%, 2%, 3%, 4%, and 5% drift for the positive loading direction are provided in Fig. 10 and Table 7 for the high-order and reduced-order models. The maximum absolute error (reduced-order relative to the high-order model) that occurred between all configurations analyzed was 8.9%, indicating that the resistance in the reduced-order model matches the higher-order model over a practical range of PT forces and walls lengths. A nearly linear relationship between moment resistance and drift is evident after decompression in Fig. 10, which is also evident in the post-decompression behavior of Specimen 2 in Fig. 5a. In Fig. 10, an increase in initial PT force has little effect on the post-decompression stiffness, but causes an increase in the decompression moment, which is also evident for Specimens 2 and 6 in Figs. 5a and 9b, respectively.

Table 7
Percent Error in Moment Resistance for High- and Reduced-Order Model in Parametric Study.

PT Force (kN)	Wall Length (m)	Drift (%)					
		0.5	1	2	3	4	5
445	1.83	2.6	0.2	−1.3	−1.5	−2.0	−1.1
	2.44	2.9	0.5	−1.0	−1.1	−1.7	−2.3
	2.74	2.4	−0.4	−1.9	−1.9	−2.1	−2.5
	3.04	2.2	−0.6	−2.5	−2.0	−2.4	−3.2
890	1.83	4.9	2.7	0.6	0.4	−0.1	−0.7
	2.44	5.5	2.9	1.0	0.6	−0.5	−1.3
	2.74	5.2	2.4	0.2	−0.3	−0.9	−1.6
	3.04	5.2	2.2	0.1	−0.8	−1.6	−2.3
1335	1.83	−5.4	4.8	3.5	3.3	2.9	3.4
	2.44	6.8	5.0	3.5	2.8	2.1	1.5
	2.74	7.5	4.9	3.0	2.4	1.2	0.4
	3.04	7.8	4.6	2.8	1.6	0.8	0.0
1779	1.83	−6.7	−7.0	1.5	0.3	−1.0	−2.1
	2.44	−7.1	−2.5	0.9	−0.8	−2.3	−3.5
	2.74	−0.7	−2.1	0.8	−0.4	−2.1	−3.5
	3.04	1.1	−1.1	1.4	−0.1	−2.1	−3.6
2224	1.83	−4.5	−3.5	2.4	1.6	0.1	−0.3
	2.44	4.2	−8.2	2.8	1.3	−0.4	−1.4
	2.74	−7.3	−6.5	2.6	1.0	−0.7	−2.1
	3.04	−8.9	−5.4	2.5	0.9	−0.8	−2.3

8. Summary and conclusions

The development and assessment of a high-order model and a reduced-order model for post-tensioned (PT) cross-laminated timber (CLT) rocking walls was described. The reduced-order model is more

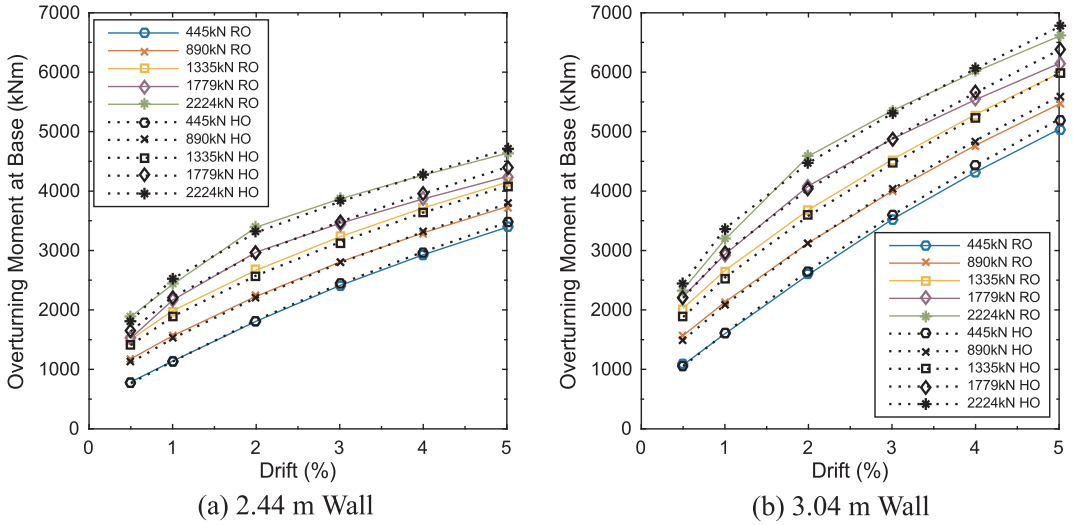

Fig. 10. Moment-Drift Reponses for High-Order Model and Reduced-Order Model for (a) 2.44 m Wall Length and (b) 3.04 m Wall Length.

computationally-efficient than the high-order model and was developed as a simplification of the higher-order model for use in nonlinear time-history analyses of buildings. The high-order model uses finite element modeling of the wall to capture local crushing deformation, stress distribution, and overall force-deformation response. The reduced-order model uses frame and link (spring) elements to capture force-deformation response. Both models were validated with data from tests on PT CLT rocking walls, including a test on coupled walls with steel U-shaped Flexural Plates (UFPs) that were modeled as inelastic shear links. Using both models, a parametric study was conducted for 20 wall configurations with varying lengths and initial PT forces. A pushover analysis was conducted to determine the load-deformation behavior of each wall in the parametric study, and results from the two models were compared. The following conclusions are drawn:

- The high-order and reduced-order model were deemed to adequately capture the force-deformation hysteretic response of existing tests on PT CLT rocking walls, including walls coupled with UFPs. Wall strength predicted from the models was within 8.3% of test data between drift demands of 1.35% and 5%.
- For PT CLT walls, the high-order model can be used to determine uplift at the base in addition to the localized stresses and strains and the extent of inelasticity (crushing) at the compression toe. Comparison of model results to existing test data indicates that the model can predict uplift within 9.3% between drift demands of 2% and 5%.
- The differences in moment resistances computed from the high-order and reduced-order model for drift demands between 0.5% and 5% were less than 8.9% over a practical range of parameters for PT CLT rocking walls.
- The force-deformation hysteresis obtained from the UPF model adequately captured the behavior measured from tests. The difference in total energy dissipation between model and test was 2.43%.
- The coupled reduced-order model captured the dissipated energy of an experimental test on coupled PT CLT rocking walls within 11% between drift cycles of 1.35% and 4%.

References

[1] FPInnovations. CLT Handbook: Cross-Laminated Timber. U.S. Department of Agriculture, Forest Service, Forest Products Laboratory, Binational Softwood Lumber Council, Canada; 2013.

[2] Sathre R, O'Connor J. A Synthesis of Research on Wood Products and Greenhouse Gas Impacts. Report No. TR-19R, Vancouver, B.C. 2010.

[3] Lineham SA, Thomson D, Bartlett AI, Bisby LA, Hadden RM. Structural response of fire-exposed cross-laminated timber beams under sustained loads. Fire Saf J 2016;85:23–34.

[4] Applied Technology Council. "Quantification of Building Seismic Performance Factors." FEMA P695, FEMA, Washington D.C; 2011.

[5] Hashemi A, Zarnani P, Masoudnia R, Quenneville P. Experimental testing of rocking cross laminated timber (CLT) walls with -resilient slip friction (RSF) joints. J Struct Eng 2018;144(1):04017180.

[6] Kelly JM, Skinner RI, Heine AJ. Mechanisms of energy absorption in special devices for use in earthquake resistant structures. Bull New Zealand Soc Earthq Eng 1972;5(3):63–88.

[7] Buchanan A, Deam B, Fragiacomo M, Pampanin S, Palermo A. Multi-storey prestressed timber buildings in New Zealand. Struct Eng Int, IABSE 2008;18(2):166–73.

[8] Hashemi A, Zarnani P, Masoudnia R, Quenneville P. Seismic resistant rocking coupled walls with innovative resilient slip friction (RSF) joints. J Constr Steel Res 2016;129(2017):215–26.

[9] Iqbal A, Fragiacomo M, Pampanin S, Buchanan A. Seismic resilience of plywood-coupled LVL wall panels. Eng Struct 2018;167:750–9. https://doi.org/10.1016/j.engstruct.2017.09.053.

[10] Priestley MJN, Sritharan SS, Conley JR, Pampanin S. Preliminary results and conclusions from the PRESSS five-story precast concrete test building. PCI J 1999;44(6):42–67.

[11] Perez F, Pessiki S, Sause R. Lateral load behavior and seismic design of unbonded post-tensioned precast concrete walls. PCI J 1999;49(2):48–64.

[12] Kurama Y, Sause R, Pessiki S, Lu L-W. Lateral load behavior and seismic design of unbonded post-tensioned precast concrete walls. ACI Struct J 1999;96(4):622–32.

[13] Kurama Y, Pessiki S, Sause R, Lu L. Seismic behavior and design of unbonded post-tensioned precast concrete walls. PCI J 1999;44(3):72–89.

[14] Perez FJ, Pessiki S, Sause R. Experimental lateral load response of unbonded post-tensioned precast concrete walls. ACI Struct J 2013;110(6):1045–55.

[15] Sarti F, Palermo A, Pampanin S. Quasi-static cyclic testing of two-thirds scale unbonded posttensioned rocking dissipative timber walls. J Struct Eng 2016;142(4).

[16] Ganey R, Berman J, Akbas T, Loftus S, Dolan JD, Sause R, et al. Experimental investigation of self-centering cross-laminated timber walls. J Struct Eng 2017;143(10).

[17] Baird A, Smith T, Palermo A, Pampanin S. Experimental and Numerical Study of U-shape Flexural Plate (UFP) Dissipators. New Zealand Society of Earthquake Engineering. 2014.

[18] Pampanin S, Priestley MJN, Sritharan S. Analytical modelling of the seismic behavior of precast concrete frames designed with ductile connections. J Earthq Eng 2001;5(3):329–67.

[19] Newcombe MP, Pampanin S, Buchanan A, Palermo A. Section analysis and cyclic behavior of post-tensioned ductile connections for multi-story timber buildings. J Earthq Eng 2008;12:83–110.

[20] Ganey R. "Seismic Design and Testing of Rocking Cross Laminated Timber Walls" MS. thesis Seattle, WA: University of Washington; 2015.

[21] Kovacs M, Wiebe L. Controlled rocking CLT walls for buildings in regions of moderate seismicity: design procedure and numerical collapse assessment. J Earthq Eng 2017.

[22] Akbas T, Sause R, Ricles JM, Ganey R, Berman J, Loftus S, et al. Analytical and experimental lateral-load response of self-centering posttensioned CLT walls. J Struct Eng 2017;143(6).

[23] Newcombe M. The connection response of rocking timber walls. New Zealand Timber Des 2015;23(1):21–8.

[24] McKenna Frank, Fenves Gredgory L, Scott Michael H. Open System for Earthquake Engineering Simulation. Pacific Earthquake Engineering Research Center. 2000.

[25] Computers Structures, Inc. "CSI Analysis Reference Manual: For SAP2000, ETABS, SAFE and CSIBridge." Computers Structures, Inc., Berkeley, CA; 2010.

[26] Horvat D. Stability Behavior of Cross Laminated Timber (CLT) Columns Under Compressive Axial Load. M.S. thesis, University of British Columbia, Vancouver, BC. 2013.

[27] ACI Innovation Task Group 5. "ITG-5.1-07 Acceptance Criteria for Special Unbonded Post-Tensioned Precast Structural Walls Based on Validation Testing." American Concrete Institute, Farmington Hills, MI; 2008.

[28] The Engineered Wood Association. "Standard for Performance-Rated Cross-Laminated Timber." APA-The Engineered Wood Association. Tacoma, WA; 2018.

[29] Dowell R, Seible F, Wilson E. Pivot hysteresis model for reinforced concrete members. ACI Struct J 1998:607–16.

[30] Structurlam. "Crosslam CLT Technical Design Guide." Structurlam; 2016.

[31] Forest Products Laboratory (FPL). Wood Handbook: Wood As An Engineering Material. (2010). Forest Products Society, Madison.

[32] Dywidag Systems International. (2006). "Dywidag Post-Tensioning Systems Multistrand Systems Bar Systems Repair and Strengthening." Dywidag.